Third-order many-body perturbation theory calculations of the ground-state energies of cesium and thallium

S. A. Blundell, W. R. Johnson, and J. Sapirstein

Department of Physics, University of Notre Dame, Notre Dame, Indiana 46556

(Received 23 April 1990)

A detailed breakdown of many-body perturbation theory contributions through third order is presented for the ground-state removal energies of cesium and thallium, with the aim of identifying which Goldstone diagrams are numerically dominant. A comparison of these diagrams with Feynman graphs is made. A discussion of the issues involved in carrying out *ab initio* calculations of properties of these atoms accurate at the few tenths of a percent level is presented.

In a recent paper[1] we addressed the question of whether or not calculating the first few orders of many-body perturbation theory (MBPT) can give accurate results for valence removal energies of cesium. Specifically, a complete calculation through third order starting with the V^{N-1} Dirac-Fock (DF) potential was carried out, and was supplemented by the calculation of two fourth-order terms for the $6s$, $7s$, and $6p$ states of neutral cesium. While the results agreed with experiment at the few tenths of a percent level, the relatively large contributions of the fourth-order terms made it obvious that a thorough investigation of that order should be made. Because there are a very large number of fourth-order terms, it would clearly be desirable to establish some criterion to judge which terms are likely to be important, and which can be safely neglected. Unfortunately, the nominal order of any given MBPT contribution is always the same, one atomic unit (a.u.), and its numerical value depends on the evaluation of a complicated sum over intermediate states and angular momentum channels weighted with various energy denominators. It is therefore difficult to tell with absolute certainty which contributions are most important without doing an explicit calculation.

What we wish to do in this paper is exhibit in detail the contributions of MBPT through third order so as to identify what kinds of term are numerically dominant, and in particular to compare a grouping of terms that arises naturally in time-dependent formulations of MBPT with one that arises naturally in time-independent MBPT. In our previous work[1] we gave only a partial breakdown of the third-order energy, which we expressed as a sum of 12 terms, where each term includes between two and eight exchange variants. The grouping together of MBPT terms that differ in only this way is equivalent to dealing with Brandow diagrams[2] instead of the Goldstone diagrams[3] of MBPT. However, there are other ways of grouping these diagrams together. An important example arises from the use of time-dependent MBPT, which is expressed in terms of Feynman graphs[4] rather than Goldstone diagrams. The mathematical expressions for Feynman graphs involve energy integrations of products of Green's functions, and appear quite different from Goldstone diagrams; however, when those integrations are carried out, any Feynman graph reduces to a set of

Goldstone diagrams. This approach has been used extensively by the Novosibirsk group in their calculations of properties of cesium.[5,6] In this paper we will show the relationship between the Feynman and Brandow groupings. While it is possible in both approaches to identify particularly important groupings, one of our principal results is that almost all groupings are sufficiently large that they cannot be neglected if results accurate to a few tenths of a percent are required. (We will, however, find for cesium a criterion that orders the size of individual Goldstone diagrams, making a limited number of them very small.) Thus, while our hope was that we could find a small subset of third-order terms which dominated, so that only the related terms of fourth and higher orders would have to be treated, we will conclude that much more complete methods are in fact required for high accuracy calculations. A discussion of such methods is given in the concluding section of this paper.

Finally, we have extended the calculations on cesium to thallium. This atom is of considerable interest for two reasons. Firstly, as is also the case for cesium,[7] a parity-nonconserving $E1$ transition matrix element $6p_{1/2} \to 7p_{1/2}$ has been measured quite precisely,[8] which has significant implications for unified theories of the weak and electromagnetic interactions.[9] Thallium is also of interest because, while nominally similar to cesium in having one electron outside filled shells, the last filled shell $6s_{1/2}^2$ is relatively weakly bound and can mix significantly with the valence $6p_{1/2}$ state, so that the behavior of perturbation theory may be quite different from that in cesium.

The plan of this paper is the following. In Sec. I, a calculation of the second-order removal energies of the ground state valence electrons of cesium and thallium with high numerical accuracy is described. The four Goldstone diagrams contributing in this order are grouped together in two different ways, one involving summing diagrams related by exchange (Brandow), and the other involving summing diagrams that are different time orderings of time-dependent MBPT (Feynman). In Sec. II, a somewhat less accurate calculation of the eighty-four Goldstone diagrams that enter in the third order is carried out, and the Brandow and Feynman groupings are compared. In Sec. III an approximate calculation of certain fourth-order diagrams is carried out,

and results compared to experiment. In this concluding section we also present an analysis of what is learned from the study of low orders of MBPT and a discussion of the role of all-orders methods in high-accuracy calculations of the properties of cesium and thallium.

I. SECOND-ORDER CALCULATIONS

We carry out our calculations starting with the $V^{(N-1)}$ DF potential. (Note that the entire calculation is relativistic, and that our perturbation theory is sometimes referred to as RMBPT, for relativistic MBPT.) There are a number of advantages associated with this potential, including a greatly reduced number of diagrams to consider, a clean separation of the core and valence states, and one set of single-particle states which can be used for calculations of excited states as well as the ground state, giving important simplifications in calculations of transition matrix elements. Thus, when considering the total energy of two different valence states of a one-valence-electron atom, that energy can be written as

$$E_v = \varepsilon_v + E_{core} ,$$ (1)

with E_{core} the same for all valence states v. Such a separation could not be made if one used, for example, unrestricted DF. Because E_{core} represents the total energy of the ion core, ε_v can be identified as the negative of the valence removal energy. In the following, because we are concerned only with the removal energies, we suppress all contributions to E_{core}. The lowest-order removal energies are, however, discrepant with experiment by -11% for both atoms. (In this and the following a positive percentage indicates the magnitude of the theoretical removal energy is larger than the experimental result, and vice versa.) Specifically, the valence $6s$ state of cesium has energy $-0.143\,10$ a.u., but $\varepsilon_{6s}^{(DF)} = -0.127\,37$ a.u. Similarly, the $6p_{1/2}$ state of thallium has energy $-0.224\,46$ a.u. compared to $\varepsilon_{6p}^{(DF)} = -0.199\,68$ a.u. Because the first-order correction to valence removal energies vanishes for a V^{N-1} DF potential, the first nonvanishing corrections are found in second order. The expression for the second order energy $\varepsilon^{(2)}$ is

$$\varepsilon^{(2)} = \alpha_1 + \alpha_2 + \beta_1 + \beta_2 ,$$ (2)

where

$$\alpha_1 = \sum_{amn} \frac{g_{vamn} g_{mnva}}{\varepsilon_{av} - \varepsilon_{mn}} ,$$ (3a)

$$\alpha_2 = -\sum_{amn} \frac{g_{vamn} g_{mnav}}{\varepsilon_{av} - \varepsilon_{mn}} ,$$ (3b)

$$\beta_1 = -\sum_{abm} \frac{g_{abmv} g_{mvab}}{\varepsilon_{ab} - \varepsilon_{mv}} ,$$ (3c)

$$\beta_2 = \sum_{abm} \frac{g_{abmv} g_{mvba}}{\varepsilon_{ab} - \varepsilon_{mv}} .$$ (3d)

In the above equations core states are denoted $a,b,c,\ldots$, excited states (which include the valence
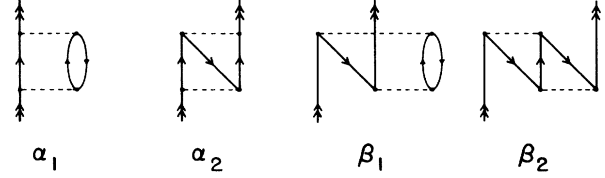

FIG. 1. Goldstone diagrams representing Eq. (3).

states v) $m,n,\ldots$, $\varepsilon_{ij} \equiv \varepsilon_i + \varepsilon_j$, and the Coulomb matrix element g_{ijkl} is defined in terms of the Dirac wave function ψ_i as

$$g_{ijkl} \equiv \int \frac{d\mathbf{r}\,d\mathbf{r}'}{|\mathbf{r}-\mathbf{r}'|} \Psi_i^\dagger(\mathbf{r})\Psi_k(\mathbf{r})\Psi_j^\dagger(\mathbf{r}')\Psi_l(\mathbf{r}') .$$ (4)

The corresponding Goldstone diagrams are shown in Fig. 1. It is possible to group α_1 and α_2, and β_1 and β_2 together because they have common denominators and one common factor in the numerator, with the second differing only by the exchange of two of the subscripts and a minus sign. Thus by introducing $\tilde{g}_{ijkl} \equiv g_{ijkl} - g_{ijlk}$ we can deal with only two objects,

$$\alpha = \sum_{amn} \frac{g_{vamn} \tilde{g}_{mnva}}{\varepsilon_{av} - \varepsilon_{mn}} ,$$ (5a)

$$\beta = -\sum_{abm} \frac{g_{abmv} \tilde{g}_{mvab}}{\varepsilon_{ab} - \varepsilon_{mv}} .$$ (5b)

This grouping together of exchange variants is equivalent to using Brandow diagrams.[2] It collects together terms with the same number of sums over core states and excited states. While the exchange graph has a distinctly different structure, especially after a radial decomposition, it is possible to evaluate the two graphs simultaneously when writing computer code: this procedure is described in an appendix of Ref. 10. However, we wish here to treat each diagram separately, and thus give in Tables I(a) and I(b) the individual values for cesium and

TABLE I. Breakdown of second-energy for (a) Cs and (b) Tl in a.u. and as percentage of total energy. Numbers in parentheses denote numerical errors.

	Energy	Percentage of total energy
	(a)	
α_1	$-0.021\,68$	15.1%
α_2	$0.002\,36$	-1.6%
β_1	$0.002\,19$	-1.5%
β_2	$-0.000\,69$	0.5%
Sum	$-0.017\,82(2)$	12.5%
	(b)	
α_1	-0.0677	30.2%
α_2	0.0113	-5.0%
β_1	0.0307	-13.7%
β_2	-0.0096	4.3%
Sum	$-0.0353(2)$	15.7%

thallium, respectively. We note first that inclusion of the second-order energy improves agreement with experiment dramatically for cesium, and somewhat less impressively for thallium, to $+1.5\%$ and $+4.7\%$, respectively. Because of the large size of the second-order effect, it is clearly important to carry out the calculation with high numerical accuracy; if an overall accuracy of 0.1% is sought, the second-order energy must be evaluated to better than 1%. Far higher numerical accuracy is achieved in the present calculation for cesium which involves a basis set of 40 wave functions for each of 22 angular momentum states, and sums over nine partial waves in the angular momentum sums, using the last partial waves to estimate the remainder of the partial wave expansion. Thallium was not evaluated as accurately, primarily because only eight partial waves were included, which made the partial wave extrapolation more uncertain. The numerical errors for the entries in Tables I(a) and I(b) do not exceed 1 in the last digit. A description of the basis set used and of how MBPT calculations are carried out with basis sets can be found in Ref. 11.

The formulas for $\varepsilon^{(2)}$ are frequently derived from Rayleigh-Schrödinger perturbation theory. If however, they are derived from a time-dependent formalism, a different grouping is more natural. In these formalisms, a central object is the single-particle Green's function, given by

$$G(\mathbf{r},\mathbf{r}';E) \equiv \sum_m \frac{\Psi_m(\mathbf{r})\overline{\Psi}_m(\mathbf{r}')}{E-\varepsilon_m+i\delta} + \sum_a \frac{\Psi_a(\mathbf{r})\overline{\Psi}_a(\mathbf{r}')}{E-\varepsilon_a-i\delta} , \quad (6)$$

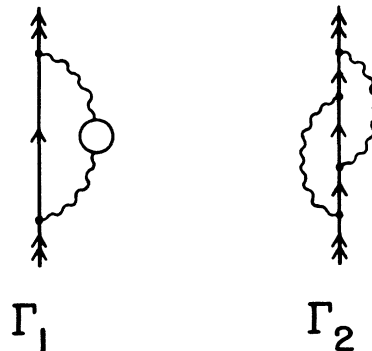where, as usual, m indicates an excited state and a indi-

FIG. 2. Feynman graphs representing Eq. (7).

cates a core state. Were we interested in the effects of negative energy states, the second term in Eq. (6) would include those states, but such effects enter in order α^3 a.u. and can be neglected here. Note that it is convenient, but not necessary, to treat excited states differently from states in the core: it is equally possible to treat all positive energy states together; the final formulas for energy shifts would be the same, but the details of the derivation slightly different. In terms of this propagator, the second-order energy can be written as the sum of two terms represented by the Feynman graphs of Fig. 2,

$$\varepsilon^{(2)} \equiv \Gamma_1 + \Gamma_2 , \quad (7a)$$

where

$$\Gamma_1 = -\int \frac{d\omega_1}{-2\pi i}\int \frac{d\omega_2}{-2\pi i}\int \frac{d\mathbf{x}\,d\mathbf{r}\,d\mathbf{x}'\,d\mathbf{r}'}{|\mathbf{x}-\mathbf{r}||\mathbf{x}'-\mathbf{r}'|}\Psi_v^\dagger(\mathbf{x}')G(\mathbf{x}',\mathbf{x};\varepsilon_v+\omega_1)\gamma_0\psi_v(\mathbf{x})\mathrm{Tr}[G(\mathbf{r},\mathbf{r}';\omega_1+\omega_2)\gamma_0 G(\mathbf{r}',\mathbf{r};\omega_2)\gamma_0] , \quad (7b)$$

$$\Gamma_2 = \int \frac{d\omega_1}{-2\pi i}\int \frac{d\omega_2}{-2\pi i}\int \frac{d\mathbf{x}\,d\mathbf{r}\,d\mathbf{x}'\,d\mathbf{r}'}{|\mathbf{x}-\mathbf{r}||\mathbf{x}'-\mathbf{r}'|}\psi_v^\dagger(\mathbf{r}')G(\mathbf{r}',\mathbf{r};\varepsilon_v+\omega_1)\gamma_0 G(\mathbf{r},\mathbf{x}';\varepsilon_v+\omega_1+\omega_2)\gamma_0 G(\mathbf{x}',\mathbf{x};\varepsilon_v+\omega_2)\gamma_0\psi_v(\mathbf{x}) . \quad (7c)$$

The rules for constructing the integrals represented by Feynman graphs are recapitulated in the appendix. Carrying out the ω integrations with Cauchy's theorem then leads to the identification $\Gamma_1=\alpha_1+\beta_1$ and $\Gamma_2=\alpha_2+\beta_2$, so that each Feynman graph reduces to a sum of Goldstone diagrams.

While at this point the Brandow and Feynman groupings give of course identical total energy shifts, it is of interest to compare their detailed breakdown. Starting with cesium we note that the Brandow organization of diagrams gives $\alpha_1+\alpha_2=-0.019\,32$ a.u. and $\beta_1+\beta_2=.001\,50$ a.u., with the twofold excited state terms (α) exceeding the single excited-state terms (β) in magnitude by a factor of 13. The Feynman organization, on the other hand, gives $\Gamma_1=-0.019\,49$ a.u. and $\Gamma_2=0.001\,67$. The close similarity between the two methods is caused by the near equality of α_2 and β_1, which is coincidental, as evidenced by their very different values in thallium. Note that exchange graphs are small and of opposite sign

to direct graphs. The most prominent feature of the Goldstone diagrams for the cesium calculation is the dominance of α_1, which is ten times larger than α_2 and β_1, and 31 times larger than β_2. Even though the latter term is relatively quite small, it still contributes 0.5% of the total removal energy, and cannot be neglected for high-accuracy work.

We can account for the ordering $\alpha_1 \gg \alpha_2$, $\beta_1 \gg \beta_2$ empirically by noting there is a suppression factor for diagrams in which the valence electron line (the set of lines starting with the initial valence line continuously connected to the final valence line, excluding loops) bends downward into a core line, which we will refer to as a "turn." This follows from the fact that a Coulomb matrix element g_{a*m*} or g_{m*a*} involves the overlap of an excited state with a core state, and that overlap is suppressed compared with the overlap of two excited states or two core states. Note however that this suppression does not appear to act in loops, even though they

also have such Coulomb matrix elements, which is why they are excluded from our definition of the valence line. This is likely because the suppression from the Coulomb matrix elements is compensated by relatively large factors coming from the angular momentum analysis. Diagram α_1 has no turns, and thus dominates the diagrams with a single turn α_2 and β_1, which in turn dominate β_2, which has two turns. We will see that this topological distinction will remain useful in the third-order calculation.

Counting the number of turns is not meaningful for Feynman graphs, which do not distinguish core and excited states. However, Feynman graphs can be categorized by how many closed electron loops are present. The dominance of Γ_1 over Γ_2 suggests that Feynman graphs with the largest number of electron loops are numerically dominant. We will see, however, that this ordering is only partially successful in third order in accounting for the magnitudes of graphs.

Turning to thallium, we see very different behavior, as might be expected from an atom that has a $6s^2_{1/2}$ core that has significant overlap with the valence orbitals. The first observation we make is that while α_1 is still the largest term, β_1 is almost half as large as α_1 rather than being ten times smaller as in the case of cesium, so that ordering of magnitudes by the number of turns in a diagram is not particularly useful for this atom. We will encounter a similar situation again in the third-order calculation; it can be understood qualitatively by noting that diagram α involves a core-valence excitation $av \rightarrow mn$, while β involves a core-core excitation $ab \rightarrow mv$. While in cesium the noble gas core is tightly bound in comparison with the valence states, in thallium the $6p_{1/2}$ valence electron interacts relatively strongly with the $6s^2$ core shell, and core-core excitations from this shell make significant contributions to the second-order ionization energy via the term β. The situation is a manifestation of the fact that the V^{N-1} DF potential is a physically more appropriate starting point for cesium than for thallium. Nevertheless, the perturbation series as a whole behaves reasonably enough for both atoms, and the formal advantages of the V^{N-1} DF potential for systematic manybody calculations make the approach a very attractive one even for thallium.

As mentioned before, α_2 and β_1 are no longer nearly equal. A remarkably feature of the second-order energy calculation for thallium is the near-cancellation between α_2 and β_2, which gives $\Gamma_2 = 0.0017$ a.u. versus $\Gamma_1 = -0.0370$ a.u. This contrasts with $\alpha = -0.0564$ a.u. and $\beta = 0.0211$ a.u. However, we will see that when we add the next-order corrections to Γ_2 this cancellation breaks down, so we attribute the smallness of Γ_2 to a numerical accident. Again, while remarkably small, it is still a 0.8% effect. It is clear that no approximation scheme that aims at the 0.1% level can leave out any graph in second order. We now turn to the third-order calculation.

II. THIRD-ORDER CALCULATIONS

Even with the elimination of a large set of Goldstone diagrams made possible by the use of the V^{N-1} DF po-

tential, there are still a large number, 84, of these diagrams contributing to the third-order valence removal energy. Of this number only 52 are independent and need be explicitly calculated, as 32 graphs are the Hermitian conjugates of other graphs. They can be obtained by reflection about a horizontal axis, and are numerically equal. We first present the formulas in the Brandow organization, which can be written as a sum of 18 terms, 12 of which are independent. Note that our arrangement of the third-order energy is somewhat different than that given in Ref. 1, with the ordering of terms different and the arrangement of the Coulomb matrix elements g systematized by having the Coulomb interaction occurring at the top of the Goldstone diagram written first, the one in the middle second, and the bottom one third:

$$E_A^{(3)} = \sum_{abmnr} \frac{\tilde{g}_{vbmr}\tilde{g}_{rabn}\tilde{g}_{mnva}}{(\varepsilon_{av} - \varepsilon_{mn})(\varepsilon_{bv} - \varepsilon_{rm})} , \tag{8a}$$

$$E_B^{(3)} = -\sum_{abcmn} \frac{\tilde{g}_{canv}\tilde{g}_{nbcm}\tilde{g}_{mvba}}{(\varepsilon_{ac} - \varepsilon_{nv})(\varepsilon_{ab} - \varepsilon_{vm})} , \tag{8b}$$

$$E_C^{(3)} = \sum_{abmnr} \frac{\tilde{g}_{avmn}\tilde{g}_{nbvr}\tilde{g}_{mrab}}{(\varepsilon_{av} - \varepsilon_{mn})(\varepsilon_{ab} - \varepsilon_{rm})} + \text{c.c.} , \tag{8c}$$

$$E_D^{(3)} = -\sum_{abcmn} \frac{\tilde{g}_{abnv}\tilde{g}_{vcbm}\tilde{g}_{nmac}}{(\varepsilon_{ab} - \varepsilon_{vn})(\varepsilon_{ac} - \varepsilon_{mn})} + \text{c.c.} , \tag{8d}$$

$$E_E^{(3)} = \sum_{amnrs} \frac{\tilde{g}_{avsr}g_{rsnm}g_{mnav}}{(\varepsilon_{av} - \varepsilon_{mn})(\varepsilon_{av} - \varepsilon_{rs})} , \tag{8e}$$

$$E_F^{(3)} = -\sum_{abcdm} \frac{\tilde{g}_{cdmv}g_{abcd}g_{mvab}}{(\varepsilon_{ab} - \varepsilon_{vm})(\varepsilon_{cd} - \varepsilon_{vm})} , \tag{8f}$$

$$E_G^{(3)} = -\sum_{abmnr} \frac{g_{abrv}g_{rvmn}\tilde{g}_{mnab}}{(\varepsilon_{ab} - \varepsilon_{vr})(\varepsilon_{ab} - \varepsilon_{mn})} + \text{c.c.} , \tag{8g}$$

$$E_H^{(3)} = \sum_{abcmn} \frac{g_{avmn}g_{bcva}\tilde{g}_{mncb}}{(\varepsilon_{av} - \varepsilon_{mn})(\varepsilon_{bc} - \varepsilon_{mn})} + \text{c.c.} , \tag{8h}$$

$$E_I^{(3)} = -\sum_{abcmn} \frac{\tilde{g}_{acmn}\tilde{g}_{vbvc}g_{mnab}}{(\varepsilon_{ac} - \varepsilon_{mn})(\varepsilon_{ab} - \varepsilon_{mn})} , \tag{8i}$$

$$E_J^{(3)} = \sum_{abmnr} \frac{\tilde{g}_{abrn}\tilde{g}_{vrvm}g_{mnab}}{(\varepsilon_{ab} - \varepsilon_{rn})(\varepsilon_{ab} - \varepsilon_{mn})} , \tag{8j}$$

$$E_K^{(3)} = -\sum_{abcmn} \frac{\tilde{g}_{vavm}g_{cban}\tilde{g}_{mncb}}{(\varepsilon_a - \varepsilon_m)(\varepsilon_{bc} - \varepsilon_{mn})} + \text{c.c.} , \tag{8k}$$

$$E_L^{(3)} = \sum_{abmnr} \frac{\tilde{g}_{vavm}g_{bmnr}\tilde{g}_{rnab}}{(\varepsilon_a - \varepsilon_m)(\varepsilon_{ab} - \varepsilon_{nr})} + \text{c.c.} \tag{8l}$$

While the Brandow form is a compact way of representing third-order perturbation theory, we now wish to consider each individual exchange diagram. To organize the presentation, we order the exchange variants of a given term in a binomial fashion. For example, for a term with three exchanges variants like $E_A^{(3)}$ we order

$$\widetilde{g}_{vbmr}\widetilde{g}_{rabn}\widetilde{g}_{mnva} = g_{vbmr}g_{rabn}g_{mnva} - g_{vbmr}g_{rabn}g_{mnav} - g_{vbmr}g_{ranb}g_{mnva} + g_{vbmr}g_{ranb}g_{mnav}$$

$$- g_{vbrm}g_{rabn}g_{mnva} + g_{vbrm}g_{rabn}g_{mnav} + g_{vbrm}g_{ranb}g_{mnva}$$

$$- g_{vbrm}g_{ranb}g_{mnav} \equiv A_1 + A_2 + A_3 + A_4 + A_5 + A_6 + A_7 + A_8 \ .$$

A similar scheme is applied to terms with two or one exchange variant, giving a set of four or two graphs. We present the diagrams in Fig. 3. Note that groups C, D, G, H, K, and L have associated complex conjugate graphs that we do not explicitly show, and that additionally $A_2 = A_5^*$, $A_4 = A_7^*$, $B_2 = B_5^*$, and $B_4 = B_7^*$. Before discussing the individual values of these diagrams, we now introduce the alternative grouping of Feynman graphs.
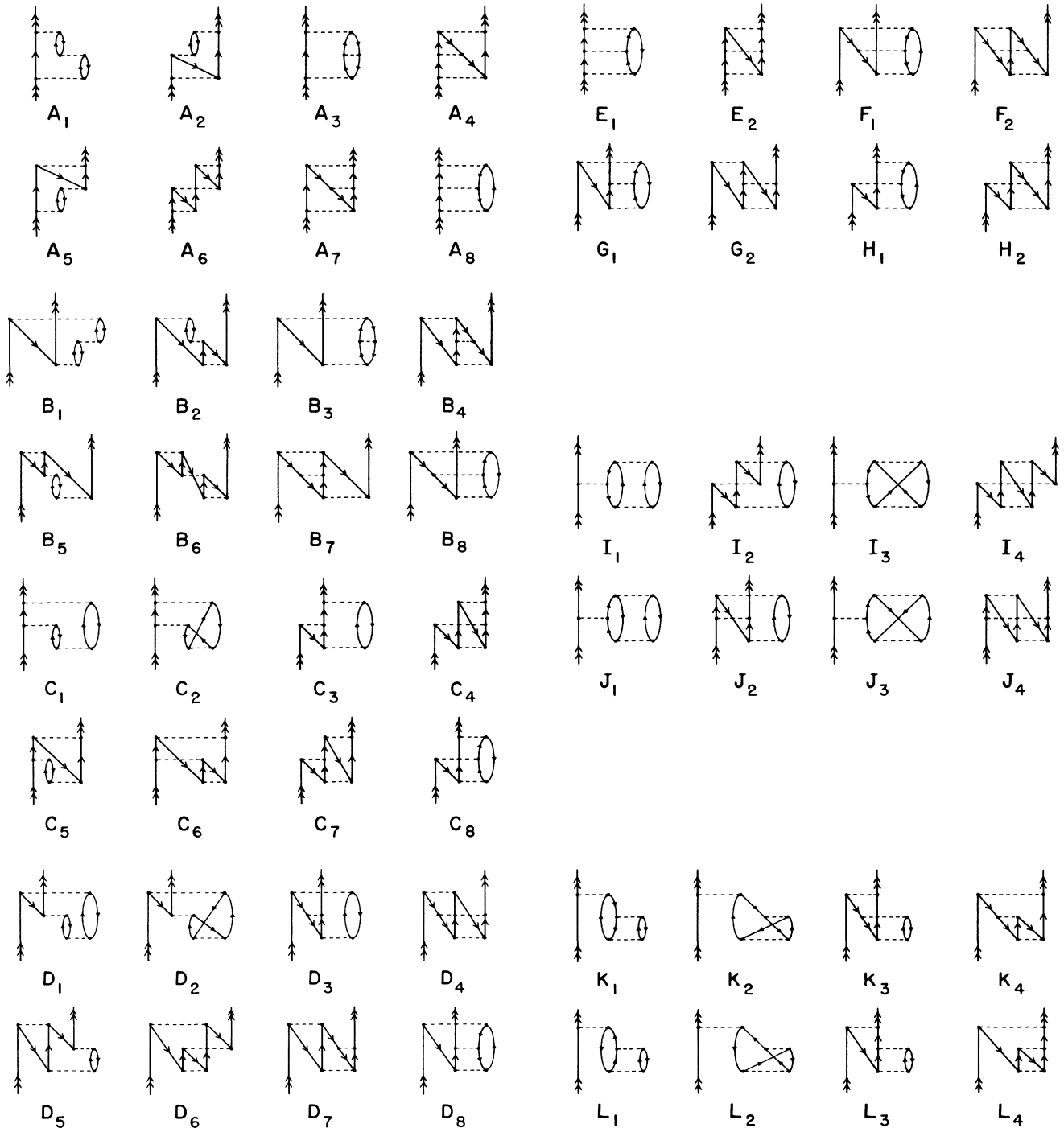

FIG. 3. Goldstone diagrams representing Eq. (8): note the ordering of exchange variants is as explained just below that equation.
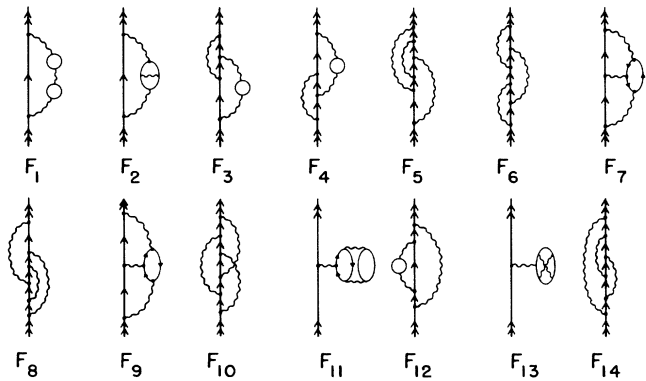
FIG. 4. Feynman graphs representing the third-order energy: see appendix for the rules for constructing the associated formulas.

In the DF potential, 14 Feynman graphs, of which 12 are distinct, must be considered. They are presented in Fig. 4; further details concerning their derivation are given in the appendix. As in the previous case, each graph is associated with several energy integrations, that when carried out with Cauchy's theorem lead to six contributions each, for again a total of 84 terms, which reproduce the Goldstone diagrams of Fig. 3. The decomposition of the Feynman graphs in terms of these diagrams is given by

$$F_1 = A_1 + B_1 + C_1 + C_1^* + D_1 + D_1^* , \tag{9a}$$

$$F_2 = A_3 + B_3 + C_2 + C_2^* + D_2 + D_2^* , \tag{9b}$$

$$F_3 = A_5 + B_2 + C_5 + C_5^* + D_3 + D_5^* , \tag{9c}$$

$$F_4 = A_2 + B_5 + C_3 + C_5^* + D_5 + D_3^* , \tag{9d}$$

$$F_5 = A_7 + B_4 + C_6 + C_4^* + D_4 + D_6^* , \tag{9e}$$

$$F_6 = A_6 + B_6 + C_7 + C_7^* + D_7 + D_7^* , \tag{9f}$$

$$F_7 = A_8 + B_8 + C_8 + C_8^* + D_8 + D_8^* , \tag{9g}$$

$$F_8 = A_4 + B_7 + C_4 + C_6^* + D_6 + D_4^* , \tag{9h}$$

$$F_9 = E_1 + F_1 + G_1 + G_1^* + H_1 + H_1^* , \tag{9i}$$

$$F_{10} = E_2 + F_2 + G_2 + G_2^* + H_2 + H_2^* , \tag{9j}$$

$$F_{11} = I_1 + J_1 + K_1 + K_1^* + L_1 + L_1^* , \tag{9k}$$

$$F_{12} = I_2 + J_2 + K_3 + K_3^* + L_3 + L_3^* , \tag{9l}$$

$$F_{13} = I_3 + J_3 + K_2 + K_2^* + L_2 + L_2^* , \tag{9m}$$

$$F_{14} = I_4 + J_4 + K_4 + K_4^* + L_4 + L_4^* . \tag{9n}$$

Note that $F_3 = F_4^*$, and $F_5 = F_8^*$ are complex conjugate pairs. As in second order, Feynman graphs collect together different exchange parts of a number of Brandow diagrams. We note here that, just as it is possible to evaluate all exchange variants simultaneously in the

TABLE II. Third-order (a) cesium and (b) thallium energies in a.u. and percentage of total energy (totals for terms C, D, G,H, K, and L are doubled to include complex conjugate terms).

	1	2	3	4	5	6	7	8	Total
					(a)				
A	0.005 579	−0.000 227	−0.006 375	0.000 469	−0.000 227	0.000 109	0.000 469	−0.004 395	3.2%
B	−0.000 344	0.000 080	0.000 363	−0.000 129	0.000 080	−0.000 027	−0.000 129	0.000 338	−0.2%
C	0.003 362	−0.000 510	−0.000 380	0.000 087	−0.000 178	0.000 039	0.000 083	−0.000 307	−3.1%
D	−0.000 260	0.000 045	0.000 311	−0.000 102	0.000 064	−0.000 018	−0.000 105	0.000 257	−0.3%
E	0.005 580	−0.000 868							−3.3%
F	−0.000 345	0.000 135							0.1%
G	−0.000 372	0.000 157							0.3%
H	0.000 184	−0.000 027							−0.2%
I	−0.074 258	0.000 410	0.018 557	−0.000 119					38.7%
J	0.074 147	−0.000 510	−0.018 519	0.000 155					−38.6%
K	−0.000 975	0.000 210	−0.000 363	0.000 092					1.4%
L	0.001 516	−0.000 306	0.000 480	−0.000 132					−2.2%
					(b)				
A	0.015 535	−0.000 666	−0.015 894	0.001 967	−0.000 666	0.000 823	0.001 967	−0.013 877	4.8%
B	−0.010 662	0.002 777	0.008 136	−0.002 737	0.002 777	−0.000 919	−0.002 737	0.007 059	−1.6%
C	0.011 092	−0.002 378	−0.002 474	0.000 880	−0.000 830	0.000 261	0.000 641	−0.001 542	−5.0%
D	−0.007 690	0.001 682	0.006 636	−0.002 392	0.002 340	−0.000 705	−0.002 486	0.006 480	−3.4%
E	0.017 882	−0.004 004							−6.2%
F	−0.007 118	0.002 681							2.0%
G	−0.008 221	0.003 194							4.5%
H	0.000 285	−0.000 014							−0.2%
I	−0.145 235	0.004 123	0.034 611	−0.001 377					48.1%
J	0.143 914	−0.007 413	−0.034 207	0.002 597					−46.7%
K	−0.005 584	0.000 828	−0.002 074	0.000 346					5.8%
L	0.008 201	−0.001 172	0.002 261	−0.000 258					−8.0%

Brandow approach, it is also possible to evaluate the Feynman diagrams directly if one carries out the energy integrals numerically instead of with Cauchy's theorem. An advantage of this approach, which has been exploited by the Novosibirsk group,[5,6] is that the important graph F_1 can be iterated to all orders relatively easily.

In Tables II and III we present the detailed breakdown of third-order perturbation theory, firstly in terms of the Brandow grouping [Tables II(a) and II(b)], and secondly in terms of the Feynman grouping [Tables III(a) and III(b)]. Unlike the case of the second-order energy, where we carried out a calculation with enough partial waves and a large enough basis set so that numerical error was under 1%, the complexity of the third-order energy calculation forces more severe approximations. The first approximation was to restrict the sum over core states to the outer, more polarizable states. Specifically, the $1s$, $2s$, $2p$, $3s$, and $3p$ states were frozen for cesium, and those states together with the $3d$, $4s$, $4p$, and $4d$ states for thallium. This approximation caused less than a 0.2% shift in the second-order energy. The second was to limit the sum over angular momentum to six partial waves for all terms except for graphs E_1 and E_2, which involve fourfold summations over intermediate states, and are by far the most computationally demanding part

of the calculation. For these we used five partial waves for the least strongly bound states and four for the more deeply bound states. No extrapolation of the tail was made. This procedure when applied to the second order energy led to a 1% error for cesium and 2% error for thallium. Finally, the last ten basis states were not summed over; this led to a negligible error in the second-order energy while saving considerable computer time. We assign an overall numerical error of 3% to the third-order energies calculated here. The first observation to make is that the total third-order energy reduces the theoretical removal energy by a relatively large amount, contributing −4.0% and −6.2% for cesium and thallium, respectively. Specifically, we find 0.0057 a.u. for cesium and 0.0140 a.u. for thallium, which actually worsens the agreement with experiment in cesium to from +1.5% in second order to −2.5% in third order, while in thallium an improvement from +4.7% in second- order to −1.6% is found. It is obvious that fourth- and possibly higher-order diagrams must be considered to achieve the tenth of a percent level; a discussion of higher orders of MBPT will be given in Sec. III.

A particularly striking feature of the third-order calculation is the extremely large size of I_1 and J_1, I_3 and J_3, which however cancel very precisely for cesium and

TABLE III. Third-order Feyman diagram energies in a.u. and percentage of total energy for (a) cesium and (b) thallium. Orderings 1–6 as in Eq. (9).

	1	2	3	4	5	6	Total
(a)							
F_1	0.005 579	−0.000 344	0.003 362	0.003362	−0.000 260	−0.000 260	−8.0%
F_2	−0.006 375	0.000 363	−0.000510	−0.000510	0.000 045	0.000 045	4.9%
F_3	−0.000 227	0.000 080	−0.000178	−0.000 380	0.000 311	0.000 064	0.2%
F_4	−0.000 227	0.000 080	−0.000 380	−0.000 178	0.000 064	0.000 311	0.2%
F_5	0.000 469	−0.000 129	0.000 039	0.000 087	−0.000 102	−0.000 018	−0.2%
F_6	0.000 109	−0.000 027	0.000 083	0.000 083	−0.000 105	−0.000 105	0.0%
F_7	−0.004 395	0.000 338	−0.000 307	−0.000 307	0.000 257	0.000 257	2.9%
F_8	0.000 469	−0.000 129	0.000 087	0.000 039	−0.000 018	−0.000 102	−0.2%
F_9	0.005 580	−0.000 345	−0.000 372	−0.000 372	0.000 184	0.000 184	−3.4%
F_{10}	−0.000 868	0.000 135	0.000 157	0.000 157	−0.000 027	−0.000 027	0.3%
F_{11}	−0.074 258	0.074 147	−0.000 975	−0.000 975	0.001 516	0.001 516	−0.7%
F_{12}	0.000 410	−0.000 510	−0.000 363	−0.000 363	0.000 480	0.000 480	−0.1%
F_{13}	0.018 557	−0.018 519	0.000 210	0.000 210	−0.000 306	−0.000 306	0.1%
F_{14}	−0.000 119	0.000 155	0.000 092	0.000 092	−0.000 132	−0.000 132	0.0%
(b)							
F_1	0.015 535	−0.010 662	0.011 092	0.011 092	−0.007 690	−0.007 690	−5.2%
F_2	−0.015 894	0.008 136	−0.002 378	−0.002 378	0.001 682	0.001 682	4.1%
F_3	−0.000 666	0.002 777	−0.000 830	−0.002 474	0.006 636	0.002 340	−3.5%
F_4	−0.000 666	0.000 277	−0.002 474	−0.000 830	0.002 340	0.006 636	−3.5%
F_5	0.001 967	−0.002 737	0.000 261	0.000 880	−0.002 392	−0.000 705	1.2%
F_6	0.000 823	−0.000 919	0.000 641	0.000 641	−0.002 486	−0.002 486	1.7%
F_7	−0.013 877	0.007 059	−0.001 542	−0.001 542	0.006 480	0.006 480	−1.4%
F_8	0.001 967	−0.002 737	0.000 880	0.000 261	−0.000 705	−0.002 392	1.2%
F_9	0.017 882	−0.007 118	−0.008 221	−0.008 221	0.000 285	0.000 285	2.3%
F_{10}	−0.004 004	0.002 681	0.003 194	0.003 194	−0.000 014	−0.000 014	−2.2%
F_{11}	−0.145 235	0.143 914	−0.005 584	−0.005 584	0.008 201	0.008 201	−1.7%
F_{12}	0.004 123	−0.007 413	−0.002 074	−0.002 074	0.002 261	0.002 261	1.3%
F_{13}	0.034 611	−0.034 207	0.000 828	0.000 828	−0.001 172	−0.001 172	0.1%
F_{14}	−0.001 377	0.002 597	0.000 346	0.000 346	−0.000 258	−0.000 258	−0.6%

somewhat less precisely for thallium. This can be traced to the Coulomb matrix elements g_{vbvc} and g_{vrvm}. When $b = c$ or $r = m$, we have the maximum possible overlap of wave functions, and thus anomalously large matrix elements. A desirable feature of the use of Feynman diagrams is that the cancellation occurs automatically, as I_1 and J_1 are summed in F_{11} [Eq. (9k)] and I_3 and J_3 in F_{13} [Eq. (9m)]. A way of understanding this cancellation is provided by the following argument, due to the Novosibirsk group.[12] Starting with terms I_1 and I_3, we note that the term g_{vbvc} reduces after a partial wave expansion to an angular factor multiplying the radial matrix element

$$R_0(vv,bc) = \langle b | V_0(vv) | c \rangle , \qquad (10)$$

where $V_0(vv)$ represents the electrostatic potential associated with the charge density of the valence electron. If we assume that this potential is a constant (as it is for $r < R$ if the valence electron charge density can be modeled by a shell of charge radius R), the summation over c is eliminated, and the resulting expression is simply the constant potential multiplying the second-order core energy. But if we make a similar argument for J_1 and J_3, the summation over r collapses in the same way, yielding exactly the same expression with a relative minus sign, leading to an exact cancellation. Of course, the actual potential of the valence electron is not exactly constant, so the cancellation is incomplete, as evidenced by the fact that $I + J$ contributes 0.1% to cesium, and 1.4% to thallium. Note that similar arguments applied to K_1, K_2, L_1, and L_2 can explain the relatively small size of these terms as a result of the vanishing overlaps that occur in g_{vavm} when the approximation that $V_0(vv)$ is constant is made.

After the large but canceling terms just discussed, the largest Goldstone diagrams for cesium are A_1, A_3, A_8, C_1, and E_1. Note that all these diagrams are perturbations to the dominant second-order Goldstone diagram α_1. From this it is clear that a very important class of fourth-order diagrams will involve second-order perturbations to α_1, a point that will be discussed further in Sec. III. Note that there is a partial cancellation between E_1 and A_8. If there were a fundamental reason for this, this would be extremely important numerically, as by far the greatest numerical problem in MBPT when finite basis sets are used is the accurate evaluation of structures like E_1, with the maximum number of excited intermediate states present. However, it is simple to argue, and we have explicitly shown by calculation, that this cancellation does not occur in the next order of MBPT, where an extra "rung" is added to the ladder structure of these diagrams. This follows from the sign rules for Goldstone diagrams: the factor of $(-1)^{n_{core}}$, where n_{core} is the number of core lines in the graph, introduces a relative minus sign between A_8, with its two core lines, and E_1, with its single core line. Addition of another rung, however, will add another core line to A_8, but leave E_1 with a single core line, leading to an additive rather than cancelling effect. Thus both diagrams and their higher-order counterparts should not be neglected for high-accuracy work.

Another notable feature of the cesium calculation is the ordering of the magnitude of diagrams by the number of "turns" as discussed in Sec. I. The large contributions explicitly mentioned above have no such turns, and the terms with two or three turns A_6, B_2, B_4, B_5, B_6, B_7, C_4, C_6, C_7, D_4, D_5, D_6, D_7, F_2, G_2, H_2, I_2, I_4, J_4, K_4, and L_4 all contribute at the 0.1% or smaller level with the exception of I_2, which although a 0.3% effect, is almost completely canceled by J_2. Particularly striking is the very small size of B_6 and D_6, which involve three turns. Thus, while empirical, this method of ordering diagrams in importance by counting how many turns are present works for both second and third order. It is quite likely that the only important fourth-order diagrams are those with zero or one turn.

Table II(a) shows that in the Brandow grouping, there is no term that does not contribute at least 0.1% of the experimental removal energy. The situation is only slightly better for the case of Feynman graphs, presented in Table III(a). As discussed in Sec. I, the size of these graphs in second order appeared to be related to the number of closed electron loops. In this way F_1 and F_{11} would be expected to be most important, followed by the set F_2, $F_3 = F_4$, F_7, F_9, F_{12}, and F_{13}, followed by $F_5 = F_8$, F_6, F_{10}, and F_{14}. We see from Table III(a) that the dominant graphs are F_1, F_2, F_7, F_9, and F_{11}. Thus this ordering is only partially successful: while it is true that all graphs contributing more than 0.5% of the experimental removal energy have one or two closed electron loops, there is a wide variation in numerical importance between graphs with the same number of loops.

At this point we are in a position to make some contact with the calculation reported in Ref. 5 on energy levels of cesium. In that work the important graphs F_1, F_2, F_3, and F_4 were treated in all-orders manner. However, the other graphs calculated here were entirely neglected. Nevertheless, a final theoretical result in agreement with experiment at the 0.1% level was obtained. While it is certainly true that the largest third-order effects are F_1 and F_2, we see that at the 0.1% level it is necessary to consider all the other graphs except for F_6 and F_{14}. Particularly important is the fact that the cancellation between F_7 and F_9, which contains the partial cancellation between A_8 and E_1 discussed previously, is imperfect, leaving a -0.5% residue. In addition F_{11}, which sums the large I and J terms of opposite signs is again relatively large, -0.7%. This is because while I and J cancel quite closely, the diagrams K and L, which are also included in F_{11}, do not. These sum to a -1.2% effect, which should have seriously spoiled the agreement between experiment and theory in the approach of Ref. 5. We thus disagree with the claim of that paper that the theoretical accuracy of their approach is under 0.3%. The good agreement obtained is presumably the result of uncalculated terms of higher-order cancelling the large third-order terms left out of the calculation.

Turning to thallium, we note that, as was the case in second order, because of the more significant mixing of the $6s^2$ core state, the argument suppressing turns breaks down significantly. For example, comparing A_1 and B_1,

which are very similar except for B_1 having a turn, a factor of 16 suppression of the latter in cesium becomes only a 1.5 suppression for thallium. Similarly, the Feynman approach changes so that while F_1 and F_2 are still the largest effects, almost every other graph contributes on the order of 1%. Therefore there is no substitute with this atom for the most complete possible calculation. Nevertheless, while there are no small contributions, neither are the calculated shifts so large that perturbation theory could be said to be out of control. What is clear, however, is that the role of higher orders of perturbation theory is crucial for accurate calculations of cesium and thallium, and we now turn to that topic.

III. HIGHER ORDERS OF MBPT

In Ref. 1, the two fourth-order Goldstone diagrams shown in Figs. 5(a) and 5(b) were calculated. They are expected to be large, being closely related to the dominant second order diagram α_1, and having no turns. In particular, the diagram of Fig. 5(a) is also enhanced by the presence of the small energy denominator associated with the line connecting the two self-energy units, which involves only the energy required to excite the valence electron. Note that we actually calculate this diagram along with an infinite set of diagrams with arbitrary numbers of self-energy units, which we refer to as "chaining" of Brueckner orbitals. The contribution of chaining is denoted by E_{BO}. Figure 5(b) was included as a member of the "ladder" series, of which $\alpha 1$ is the diagram with two rungs, E_1 the diagram with three rungs, and this diagram the member with four rungs. We denote its value by $E_{ladder}^{(4)}$. The previous results for cesium were $-0.002\,69$ a.u. for E_{BO} and $-0.001\,01(20)$ for $E_{ladder}^{(4)}$, which when added to the previous calculations leads to agreement with experiment at the 0.1% level. We have carried out a similar calculation for thallium with the result $0.000\,37$ a.u. for E_{BO} and $-0.003\,26(60)$ a.u. for $E_{ladder}^{(4)}$, which gives agreement with experiment at the 0.2% level. This is within the 0.3% theoretical error forced by the very rough calculation of $E_{ladder}^{(4)}$, which restricted the core to $6s$, $5d_{3/2}$, and $5d_{5/2}$, with only three partial waves included for $6s$ and two for the $5d$ states. The small value of E_{BO} is rather fortuitous, for closer investigation reveals that it occurs principally because of a cancellation between the contribution from chaining on excited lines [as shown in Fig. 5(a)], and the contributions from chaining on core lines and from associated folded diagrams. We summarize in Tables IV(a) and IV(b) the MBPT results calculated in this paper for the ground-state energies of Cs and Tl.

We would like to stress that inclusion of E_{BO} and $E_{ladder}^{(4)}$, while successful in getting agreement with experiment at the few tenths of a percent level, in no sense represents a complete calculation of fourth order. As with the case of Ref. 5, the good agreement with experiment simply means that the remainder of uncalculated terms cancel fairly precisely. What is really necessary is a full calculation of higher order terms. We have in the remaining diagrams of Fig. 5 and in Figs. 6 and 7
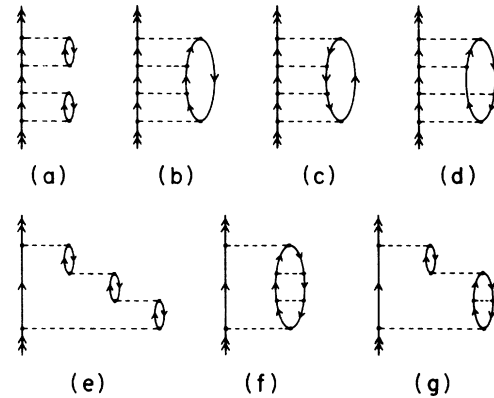

FIG. 5. Representative fourth-order Goldstone diagrams picked up by singles-doubles all-orders methods.

presented a representative set of Goldstone diagrams that we consider likely to play an important role in high accuracy calculations. As with Figs. 5(a) and 5(b), they are all perturbations on α_1 and have no turns. We have already discussed Fig. 5(c) in Sec. II, and showed that it has the same sign as Fig. 5(b), so that the partial cancellation exhibited between their third-order counterparts, A_8 and E_1 no longer takes place. In fact, for thallium the value of Fig. 5(c) is $-0.0037(5)$ a.u., somewhat larger than $E_{ladder}^{(4)}$. As the inclusion of this diagram leads to disagreement with experiment at the 1.5% level, we certainly cannot claim understanding of this atom at the few tenths of a percent level. In order to reach this level, the diagrams that cancel this large effect must be identified, and some method found to justify neglect of uncalculated diagrams in fourth and higher orders.

The most direct way to approach this problem is to carry out the procedure of this paper for MBPT through fourth order. While this is a very large scale task, the increasing algebraic and numerical power of computers

TABLE IV. Behavior of low orders of MBPT for (a) Cs and (b) Tl, in units of a.u. Numbers in parentheses denote numerical errors.

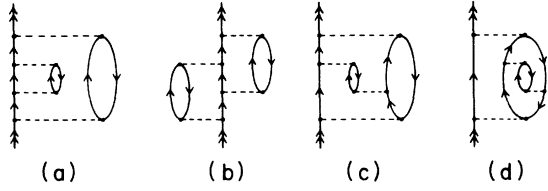| Order	Energy	Accumulated energy
	(a)	
0th	$-0.127\,37$	$-0.127\,37$
2nd	$-0.017\,82(2)$	$-0.145\,19(2)$
3rd	$0.005\,70(17)$	$-0.139\,49(17)$
4th (partial)	$-0.003\,70(20)$	$-0.143\,19(26)$
		$-0.143\,10$ (Expt.)
	(b)	
0th	-0.1997	-0.1997
2nd	$-0.0353(2)$	$-0.2350(2)$
3rd	$0.0140(4)$	$-0.2210(4)$
4th (partial)	$-0.0029(6)$	$-0.2239(7)$
		-0.2245 (Expt.)

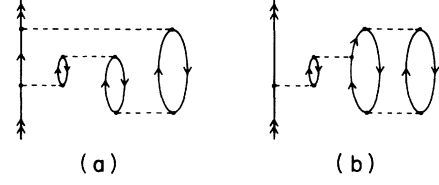FIG. 6. Representative fourth-order Goldstone diagrams involving triple excitations.

FIG. 7. Representative fourth-order Goldstone diagrams involving coupled-cluster effects.

make it likely that it can be successfully carried out. However, the use of all-orders methods provides an alternative method of investigation that automatically includes large classes of fourth-order MBPT, while also

summing infinite classes of higher-order terms. As an example of such a method, we repeat from Ref. 13 a set of coupled equations that represent one all-orders method we refer to as the singles-doubles, or SD method:

$$(\varepsilon_a - \varepsilon_m)\rho_{ma} = \sum_{bn} \rho_{nb}\tilde{g}_{mban} - \sum_{bcn} g_{bcan}\tilde{\rho}_{mnbc} + \sum_{bnr} g_{mbnr}\tilde{\rho}_{nrab} \, , \tag{11a}$$

$$(\varepsilon_v - \varepsilon_m + \delta E_v)\rho_{mv} = \sum_{an} \rho_{na}\tilde{g}_{mavn} - \sum_{abr} g_{abvr}\tilde{\rho}_{mrab} + \sum_{anr} g_{manr}\tilde{\rho}_{nrva} \, , \tag{11b}$$

$$(\varepsilon_{av} - \varepsilon_{mn} + \delta E_v)\rho_{mnva} = g_{mnva} + \sum_{rs} g_{mnrs}\rho_{rsva} + \sum_{bc} g_{bcva}\rho_{mnbc} + \sum_r \rho_{ra}g_{nmrv} + \sum_r \rho_{rv}g_{mnra}$$

$$- \sum_b \rho_{nb}g_{bmav} - \sum_b \rho_{mb}g_{bnva} + \sum_{br} \tilde{g}_{bmrv}\tilde{\rho}_{nrab} + \sum_{br} \tilde{g}_{bnra}\tilde{\rho}_{mrvb} \, , \tag{11c}$$

$$(\varepsilon_{ab} - \varepsilon_{mn})\rho_{mnab} = g_{mnab} + \sum_{rs} g_{mnrs}\rho_{rsab} + \sum_{cd} g_{cdab} \rho_{mncd} + \sum_r \rho_{rb}g_{nmra} + \sum_r \rho_{ra}g_{mnrb}$$

$$- \sum_c \rho_{nc}g_{cmba} - \sum_c \rho_{mc}g_{cnab} + \sum_{cr} \tilde{g}_{cmra}\tilde{\rho}_{nrbc} + \sum_{cr} \tilde{g}_{cnrb}\tilde{\rho}_{mrac} \, , \tag{11d}$$

$$\delta E_C = \tfrac{1}{2} \sum_{abmn} \tilde{g}_{abmn}\rho_{mnab} \, ,$$

$$\delta E_v = \sum_{amn} g_{vamn}\tilde{\rho}_{mnva} + \sum_{abm} g_{abvm}\tilde{\rho}_{mvab} + \sum_{ma} \tilde{g}_{vavm}\rho_{ma} \, . \tag{12}$$

These can be obtained fairly directly by applying the Schrödinger equation to the wave function (with the neglect of the last two terms, which are discussed later),

$$|\Psi_v\rangle \equiv N_v \left[1 + \sum_{am} \rho_{am}a_m^\dagger a_a + \tfrac{1}{2} \sum_{abmn} \rho_{mnab}a_m^\dagger a_n^\dagger a_a a_b + \sum_m \rho_{mv}a_m^\dagger a_v + \sum_{amn} \rho_{mnva}a_m^\dagger a_n^\dagger a_a a_v \right.$$

$$\left. + \left[\tfrac{1}{2} \sum_{abmnr} \rho_{abvmnr}a_m^\dagger a_n^\dagger a_r^\dagger a_a a_b a_v + \tfrac{1}{6} \sum_{abcmnr} \rho_{abcmnr}a_m^\dagger a_n^\dagger a_r^\dagger a_a a_b a_c \right] \right] a_v^\dagger |O_C\rangle \, . \tag{13}$$

By dropping all ρ terms on the right-hand side of Eq. (11), a lowest-order expression for ρ_{mnab} and ρ_{mnva} can be obtained, that, when used in Eq. (12) reproduces Eq. (3). However, when the next iteration is performed, it is straightforward to show that this method, although it sums an infinite class of diagrams, misses the complex conjugate terms in $E^{(3)}$ along with diagrams I and J. On the other hand, it can also be shown that on the next iteration, every diagram of Fig. 5 *is* accounted for by the SD method. Thus a very complete calculation can be carried out by solving the above equations, and accounting for the missed third-order terms explicitly in perturbation theory.

As is planned to be reported in another publication,[14]

this very complete calculational method when applied to cesium still leads to disagreement with experiment by -0.5%. We believe that the graphs of Figs. 6 and 7 are responsible for this discrepancy. They have to do with what we call "triples," and "coupled-cluster" terms, respectively. Figure 6(a) is a self-energy correction to an internal excited line in the second-order self-energy; because the second-order self-energy constitutes a relatively large modification of the DF potential, it is possible that this effect enters at the several tenths of a percent level. The reason for the nomenclature "triples" can be seen by drawing a horizontal line through the middle of the diagram: the associated energy denominator involves the sum of three excited states. While the SD method cannot

account for this diagram, it is possible to modify the method by including the terms in large parentheses in Eq. (13). When these terms are included, a new equation for them is obtained, and they enter in addition on the right-hand sides of the equations for ρ_{mv} and ρ_{mnva}. These modifications restore the missed third-order terms, and in fourth order lead to the new contributions shown in Fig. 6. Note that Figs. 6(c) and 6(d) are examples of third-order diagrams in which a Coulomb interaction has been replaced by one containing a ring. By analogy with the effect on diagram α_1, this insertion of rings (to all orders) may lead to a modification of the strength of the Coulomb interaction by a factor of about $\frac{1}{3}$, as pointed out by the Novosibirsk group. In that case, Fig. 6(d) would enter at over 1%, and Fig. 6(c) at the several tenths of a percent level. For this reason, if an all-orders approach is to be used for accurate calculations of cesium and thallium, we think it essential that triples be accounted for in some fashion.

The last diagrams we wish to discuss are the coupled-cluster diagrams of Fig. 7. These contain quadruple excitations which can be factorized into a product of double excitations, and can be accounted for by inclusion of non-linear terms $(1/2!)$ S_2^2, where S_2 represents a double excitation. Effects of the nonlinear term $S_1 S_2$, where S_1 represents a single excitation also enter in fourth order: we expect these terms to enter at the tenth of a percent level.

The main purpose of this paper has been to exhibit in detail the workings of MBPT in Brandow and Feynman form through third order for cesium and thallium. With regard to the question of just what kind of calculation is necessary to truly reproduce with high accuracy the spectra of these extremely complex atoms, we consider the point open. While it is very likely that some sort of all-orders method will be necessary for this purpose, we believe that it is of great value to examine as thoroughly as possible the behavior of MBPT in the first few orders so as to provide a guide to what an all-orders method picks up, and what effects it neglects. Regardless of the apparent power or beauty of such a method, if numerically significant diagrams of low order are missed, any agreement with experiment is clearly fortuitous. It is very likely, however, that any all-orders method that is powerful enough to account for all the second and third order terms calculated here, along with the diagrams shown in

Figs. 5, 6, and 7, will provide an extremely accurate method for calculating the properties of these atoms.

APPENDIX: FEYNMAN DIAGRAM FORMULAS

In this appendix we explain how to derive the formulas for the energy shifts associated with Fig. 4, and how these in turn can be related to Goldstone diagrams as done in Eq. (9). More details can be found in Ref. 4. Consider the graph F_1. Associate a radial variable with each vertex. A photon line connecting points r_i and r_j is associated with a Coulomb interaction $1/|r_i - r_j|$. (Strictly speaking, we are working in Coulomb gauge and making the approximation of dropping the transverse part of the photon propagator: note also we suppress the fine-structure constant.) The next step is to assign energies to each line, conserving energy at each vertex. The initial electron in our example has energy ε_v: we choose to send off energy ω_1 through the photon line, which leaves the electron with energy $\varepsilon_v - \omega_1$. If we choose the radial variables so that the electron travels from r_1 to r_6 with this energy, that line is to be associated with the electron propagator $G(r_6; r_1; \varepsilon_v - \omega_1)$. While the photon lines carry energy, note that the Coulomb part of their propagators does not have any dependence on this energy, although the transverse part we are neglecting does. The photon energy ω_1 is then augmented in our example by ω_2 carried by one of the electron lines in the first closed electron loop, which forces the other electron to have energy $\omega_1 + \omega_2$. The following photon again has energy ω_1, which is augmented by ω_3 in the second loop. Each energy is integrated over with a factor of $(-2\pi i)$ in the denominator, a factor of γ_0 associated with each vertex, a factor of (-1) inserted and a trace taken over each closed electron loop, and finally all radial variables are to be integrated over, and the entire expression sandwiched between $\bar{\psi}_v(r_6)$ and $\psi_v(r_1)$ to get the Feynman integral for the associated energy shift,

$$F_1 = \int \frac{d\omega_1}{-2\pi i} \int \frac{d\omega_2}{-2\pi i} \int \frac{d\omega_3}{-2\pi i} \int \frac{dr_1 dr_2 dr_3 dr_4 dr_5 dr_6}{|r_1 - r_2||r_3 - r_4||r_5 - r_6|} \psi_v^\dagger(r_6) G(r_6, r_1; \varepsilon_v - \omega_1)$$

$$\times \gamma_0 \psi_v(r_1) \text{Tr}[G(r_5, r_4, \omega_1 + \omega_3) \gamma_0 G(r_4; r_5; \omega_3) \gamma_0] \text{Tr}[G(r_3, r_2, \omega_1 + \omega_2) \gamma_0 G(r_2, r_3; \omega_2) \gamma_0] . \quad (A1)$$

The connection with Goldstone diagrams given in Eq. (9) is obtained either by expressing the Green's functions using Eq. (6) and directly carrying out the ω integrations with Cauchy's theorem or, more simply, by using a graphical algorithm in which one generates systematically all time orderings of a given Feynman diagram.[15] Schematically, one associates each photon line of a Feyn-

man diagram with a number. One then distorts each diagram thus labeled so that the photon lines are horizontal and in the 3!=6 possible orderings. The electron lines will then have a definite orientation, up or down, and the usual Goldstone rules of associating upward going lines with excited states and downward with core states can be applied to give the results of Eq. (9).

[1]S. A. Blundell, W. R. Johnson, and J. Sapirstein, Phys. Rev. A **38**, 4961 (1988).

[2]B. H. Brandow, Rev. Mod. Phys. **39**, 771 (1967).

[3]J. Goldstone, Proc. R. Soc. London Ser. A **239**, 267 (1957).

[4]A. Fetter and J. D. Walecka, *Quantum Theory of Many-Particle Systems* (McGraw-Hill, New York, 1971).

[5]V. A. Dzuba, V. V. Flambaum, and O. P. Sushkov, Phys. Lett. A **140**, 493 (1989).

[6]V. A. Dzuba, V. V. Flambaum, A. Ya. Kraftmakher, and O. P. Sushkov, Phys. Lett. A **142**, 373 (1989).

[7]M. C. Noecker, B. P. Masterson, and C. E. Wieman, Phys. Rev. Lett. **61**, 310 (1988).

[8]P. Drell and E. D. Commins, Phys. Rev. A **32**, 2196 (1985).

[9]U. Amalidi *et al.*, Phys. Rev. D **36**, 1385 (1987).

[10]W. R. Johnson, S. A. Blundell, and J. Sapirstein, Phys. Rev. A **37**, 2764 (1988).

[11]W. R. Johnson, S. A. Blundell, and J. Sapirstein, Phys. Rev. A **37**, 307 (1988).

[12]O. P. Sushkov (private communication).

[13]S. A. Blundell, W. R. Johnson, Z. W. Liu, and J. Sapirstein, Phys. Rev. A **40**, 2233 (1989).

[14]S. A. Blundell, W. R. Johnson, and J. Sapirstein (unpublished).

[15]This procedure is implicit in the discussion on pp. 111–116 of Ref. 4.